Mechanical and Biological Properties of Chitosan Nanocomposite Films: Effects of POSS nanoparticles

R. VENKATESAN*, S. R. DARSON IMMANUEL JOHN AND N. RAJESWARI

*College of Engineering Guindy, Anna University,
Chennai, Tamil Nadu, India-600025*

ABSTRACT

Nanocomposite films of chitosan (CH) incorporated with different wt. % of the polyoligomericsilsesquioxane (POSS) were prepared by solution casting. The thermal, mechanical, morphological and antimicrobial properties of the nanocomposites were examined. TGA analyses of the nanocomposites indicate that the filler enables the enhancement of thermal stability of chitosan. The tensile strength of the nanocomposite films is enhanced (10.9 MPa for neat chitosan to 24.0MPa for 5wt. % filled chitosan) by the addition of POSS while the elongation at break is reduced. The nanocomposite films exhibited excellent antimicrobial activity against both gram positive and gram negative bacteria. This activity increases with increasing filler content. Chitosan as well as POSS (the organic part) are biodegradable and hence these nanocomposite films can find application as food packaging material given their flexibility.

KEYWORDS: *Biodegradable Chitosan, POSS, Nanocomposites, Mechanical strength, Food packaging*

INTRODUCTION

The most widely using and lavish commodity plastics such as polyethylene (PE), polypropylene, polystyrene and poly (vinyl chloride) are omnipresent plastics in the environment, rising problematic categories of soil and water wastes. Owing to the increasing scarcity of petroleum resources coupled with the continual worsening of global "white pollution," the study of biodegradable bio-based materials paid more attention for researchers all around the world. Recently, renewable, green polymeric material, bio composites have intrigued as a novel class of materials. There

has been a huge growth in the development of bio-degradable plastics to diminish the environmental sway of the disposal of conventional oil-based plastics. Such bio-based polymers are also bio-degradable, and also reduce carbon footprint.

However, biodegradable polymers represent a very interesting alternative to the replacement of synthetic plastic packaging materials, [1-3] especially for use in food packaging[4] within the family of biodegradable polymers. Recently, biopolymers from various natural resources have been used as eco-friendly packaging materials to substitute the non-biodegradable, petroleum-based plastic based packaging materials. Biodegradable polymers (BPs) offer a number of advantages to environmental conservation due to their non-harmful effects. They can be classified into two major categories: natural polymers and synthetic polymers. Natural polymers include cellulose [5–8] chitin and chitosan [9–11] and other essential macromolecules such as proteins.[12-13]

Chitosan is a polymer obtained from dc acetylation of chitin, is a cationic polysaccharide with linear chain consisting of β-(1,4)-linked 2-acetamino-2-deoxy-β deglucopyranose and 2-amino-2-deoxy-β-D-glucopyranose. Chitosans are used in dietary supplements, water treatment, food preservation, agriculture cosmetics, pulp & paper and medicinal application. This is due to its biocompability, biodegradability, non-toxicity, and other unique properties such as film ability, chelation and adsorption properties and antimicrobial activity.

Currently Polyhedral oligomericsilsequioxane (POSS) incorporated nanocomposites are emerging as a new chemical technology in processing of materials. POSS molecules are derived by the hydrolysis and condensation of trifunctionalorganosilanes and possess the structure of cube-octameric frameworks. The structure of POSS is represented by the formula $R_n(SiO_{1.5})_n$, where n=6-12 and R denotes various organic corner groups, one or more of which is polymerizable or reactive in the inorganic silica-like core. The incorporation of POSS molecules in the polymer matrices allows the construction of materials with precise control over the nanoarchitecture to impart ease of processing and excellent properties. POSS is an attractive and ideal building block for the synthesis of new organic-inorganic hybrid materials. Embedding functionalized POSS in the polymer matrix not only leads to the enhancement of electrical properties [14] and thermal stability[15] due to their unique characteristics, but also improves their biocompatibility as well.[16-18] There are few reports on soluble nano particles prepared from gold, copper, cobalt, platinum and silica. Functionalization of POSS also leads to better distribution in the polymer by covalent interactions, enables higher miscibility with the polymer resulting in better solubility in the cured network, which improves the properties, significantly.[19-21] Here, both PBAT and Cl-POSS are soluble in dichloromethane (DCM). The structure of the specific POSS used in this work, octakis (3-chloropropyl) octasilsesquioxane is shown in Scheme 1.

There are few recent studies on biodegradable composites consisting of nano-fillers and prepared by solution casting method.[22-23] Addition of POSS-NH3+ with gelatin was a
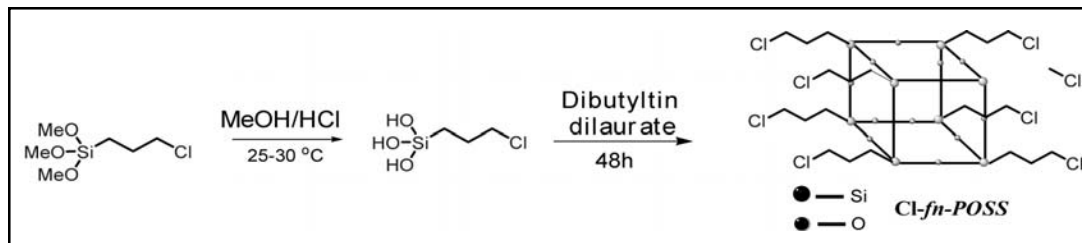
SCHEME 1. Synthesis of octakis(3-chloropropyl)silsesquioxane(Cl-fn-POSS).

powerful tool for the modulation of mechanical and biological features of ionic hydrogels, making those new composites family suitable for biomedical applications in the soft tissue engineer ref. Keratin fibers have been nanoreinforced by grafting of polyhedral oligomericsilsesquioxanes (POSS) nanocages by exploiting the reactive functional groups (–SH, –NH$_2$, –COOH, –OH) present on the fiber surface.

POSS is an attractive and ideal building block for the synthesis of new organic-inorganic hybrid materials. Embedding functionalization POSS in the polymer matrix not only leads to the enhancement of electrical properties[24] and thermal stability[25] due to their unique characteristics, but also improves their biocompatibility as well.[26-28] Fictionalization of POSS also leads to better distribution into the polymer by covalent interactions.[29-31] There are few recent studies on biodegradable composites consisting of nano-fillers and prepared by solution casting method.[32-33]

The objective of the present study was to develop chitosan films containing different wt. % of POSS by solution casting. The interest of this study comprises active and functional food packaging. For this purpose, the influence of the casting process on antimicrobial activity of chitosan nanocomposites, their mechanical, thermal, barrier and morphological properties were investigated.

EXPERIMENTAL

Materials

Commercial grade chitosan powder was purchased from the SRL, Mumbai, India. (3-chloropropyl) trimethoxysillane (97 %) was purchased from Alfa Aesar, India. Methanol (99%), acetic acid were purchased from Sigma Aldrich, India. All chemicals were used as received without further purification.

Synthesis of POSS nanoparticles

POSS was synthesized as per earlier procedure.[16] A solution of 150mL of methanol, 5mL of con. HCl was placed in a two necked round bottom flask equipped with condenser and a Teflon coated magnetic pellet. The mixture was stirred for 30 minutes at 25-30 °C. To this solution, 30 g (0.075 mol) of (3-chloropropyl) trimethoxysilane was added drop-wise over a period of 30 min through an addition funnel while it was stirred vigorously. The stirring was continued up to 2 h. Subsequently it was placed at room temperature without stirring for complete hydrolysis of the methoxy group for 48 h. Subsequently, di-*n*-butyl tin dilaurate (0.30 g, 0.024 mol) catalyst was added for self-condensation of the Si-OH groups. The reaction mixture was maintained for another 2 days at room temperature upon which a white crystalline solid was obtained as a precipitate.

Preparation of chitosan nanocomposites

Neat chitosan and CH/POSS nanocomposites were developed by the solution casting method as described

earlier.[36] 2.0g of chitosan was mixed with different weights of POSS (such that the final wt.% 0.5, 1.0, 3.0 and 5.0 wt.%, respectively) in a beaker equipped with a magnetic pellet. 2.5mL of acetic acid was added and the mixture was stirred (using magnetic stirrer; REMI, India) at 25-30 °C with continuous stirring until it is dissolved completely (typically for 30 min) to form a homogeneous film forming solution (FFS). The control (neat CH film) was also prepared by using acetic acid without POSS. The FFS was then poured into a glass Petridish (80 x 15 mm). It was allowed to dry overnight under ambient conditions followed by drying around 40 °C for 24 h in an oven. The dried film

was removed from the petridish using a spatula, placed in a sealed airtight plastics bag, and stored at room temperature until further analysis. The sample nomenclature and details are shown in Table 1.

Characterization

Fourier transform infrared (FT-IR) spectra of the films were measured using a Fourier transform infrared (FTIR) spectrophotometer (Bruker Alpha Model, India). The spectral window was between 4000-500 cm^{-1} with the line resolution being 4 cm^{-1}. Film samples were cut into rectangular shape (5 × 5 cm) and used directly. XRD measurements were performed using Bruker D8

TABLE 1. Chitosan/POSS compositions Prepared and their nomenclature

S. No	Nomenclature	Chitosan (g)	Nano Choloro-POSS (g)	
			% of CH	NPs
1.	A	2.0	2.00	0.00
2.	B	2.0	1.99	0.01
3.	C	2.0	1.98	0.02
4.	D	2.0	1.94	0.06
5.	E	2.0	1.90	0.10

Advance (Germany) x-ray diffractometer and the diffraction pattern was recorded between 2θ values of 10 to 80 degrees. The wavelength (λ) of the incident CuK$_\alpha$ radiation was 1.54 Å and the scanning rate was 0.05° s^{-1}(from 2θ = 10° to 80°). The scanning electron microscopy (SEM) images of the film samples and POSS were obtained using an electron microscope JEOL model JSM-5000 operated at 10.0 kV. All samples were sputter coated with a thin layer of gold prior to analysis in order to increase their electrical conductivity. TEM analysis was carried out with FEI Tecnai T20 Electron Microscope at an acceleration voltage of 200 kV. A solution with POSS and chloroform was prepared and subjected to ultra sonication for 30 min to complete dissolution. A drop of this solution was placed onto 300 mesh Cu grid and air-dried. In the case of CH and POSS mixtures, the solution prepared was dip-coated onto the Cu grid and air-dried before analysis. The thermal stability evaluation was carried out using TA Instruments Q500 Hi-Res

(Thermogravimetric analyzer) TGA. All the TGA analysis were performed in the temperature window 35 to 800 °C at the scanning rate of 20 °C min^{-1} under nitrogen atmosphere (nitrogen flow rate was 60 mL min^{-1}). The differential scanning calorimetry (DSC) was performed with Thermal Analyst (make, model, county). All the DSC runs were conducted with the heating rate being 20 °C min^{-1}. Mechanical properties such as tensile strength (TS), elongation at break (EAB), and tensile modulus (TM) of each sample was evaluated using a Universal Testing Machine (UTM, H10KS, Tinius Olsen, UK) in accordance with the ASTM standard method D 882-88. The gauge length of each film used in the testing was 50 mm. The rate of elongation was uniformly, 500 mm/min. The water vapor permeability (WVP) of nanocomposites was determined gravimetrically following the ASTM E96-95 standard (Reddy and Rhim 2014). Films were cut into round shape and directly placed on the top of cups containing 20 mL of water

and sealed tightly. The assembled cup was weighed and subsequently placed in a humidity chamber controlled at 25 °C and 50% RH. Weight change of the cup was determined at every 1 h for 8 h. The slopes of the steady-state portion of weight loss versus time curves were used to calculate the water vapor transmission rate (WVTR; g/m^2s) of the film. Then, the WVP (g/m^2 s Pa) of the film was calculated as follows:

$$WVP = \frac{WVTR \times L}{\Delta p}$$

Where L is the mean thickness of the film (m) and Δp is the partial water vapor pressure difference (Pa) across the film. OTR of the PBAT and PBAT nanocomposite films was calculated by oxygen permeability tester (Noselab Ats, Italy) at 25°C under the condition of 0% RH at 1 atm according to ASTM D-3985 standard. The measurements were taken three times at different places of the film and the average value was calculated. All specimens were conditioned at ambient conditions. The antimicrobial activities of the neat CH and its nanocomposites were examined by the zone of inhibition method. Food pathogenic bacteria, *E.coli* and *S.aureus* are used for testing the antimicrobial activity of the films. For the qualitative measurement of antimicrobial activity, the film samples were punched to make disks (diameter = 10 mm), and the antimicrobial activity was determined using a modified agar diffusion assay (disk test). The plates were examined for possible clear zones after incubation at 37°C for 2 days. The presence of any clear zone that formed around the film disk on the plate medium was recorded as an indication of inhibition against the microbial species.

RESULT AND DISCUSSION

Characterization of CH and CH/POSS nanocomposites

Infrared Spectroscopy

FTIR spectra were obtained for the initial chitosan and synthesized composite (Figure 1). In the FTIR spectrum of chitosan, the band at 3429 cm^{-1} corresponds to the stretching vibrations O-H of hydroxyl groups bound with carbon atoms. Intensive absorption bands at 2800 to 3000 cm^{-1} are observed due to the C-H stretching vibrations. The band at 1580 cm^{-1} corresponds to the deformation vibrations of -NH_2; 1420 and 1380 cm^{-1} for C-H bending vibrations, 1310 cm^{-1} for asymmetric C-O-C stretching vibrations, and 1080 cm^{-1} for C-O stretching vibration of CH-OH were observed.

X-ray diffraction Analysis

Figure 2 is a presentation of the XRD analysis carried out to characterize the phase structure of CH/POSS nanocomposites. From the diffractogram, the peak most prominent amorphous curve is observed at 22.9° in the 2θ angle which shows the amorphous state of the silica network whereas the chitosan exist as an anhydrous crystalline phase. Todorova et al., 2014, Kow et al., 2014 reported anhydrous crystalline chitosan and amorphous POSS of silica respectively at $2\theta = 23°$. A highly discrete crystalline projection found at 2θ angle of 29.3° shows the contribution of the silica phase. All these observations suggest that no significant changes take place in the crystal structure of CH upon the addition of POSS as nanofiller.

Morphological Properties

All the films formed, including pure CH and CH/POSS nanocomposite films were flexible and free-standing. The SEM images PBAT/POSS films are presented in Figure 3. The POSS aggregates were plate-like in appearance. The neat CH films exhibited a smooth, compact and homogeneous surface. The presence of pseudo sperical particles of size around 5 to 8 μm, possibly arising due to coating of PBAT around the filler is evident in the case of nanocomposite films containing POSS is
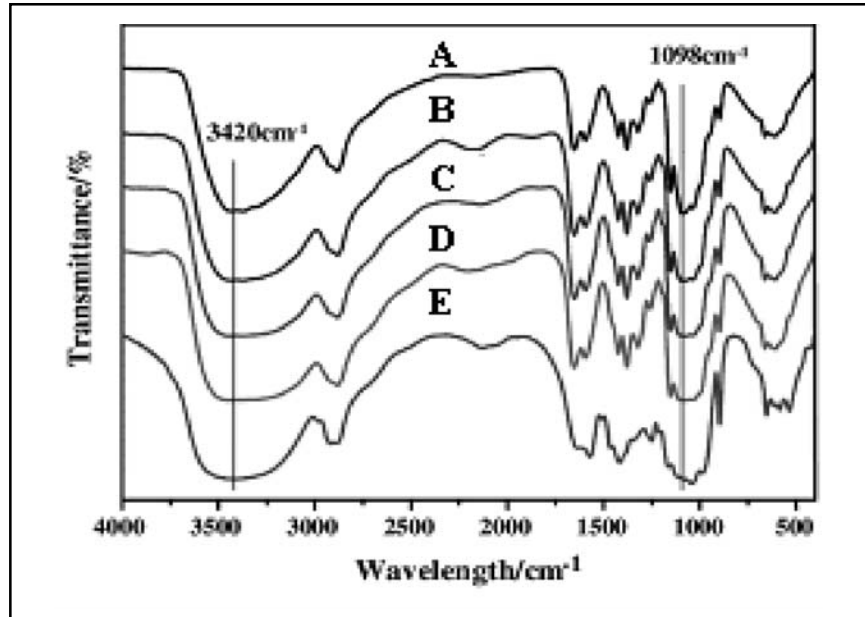
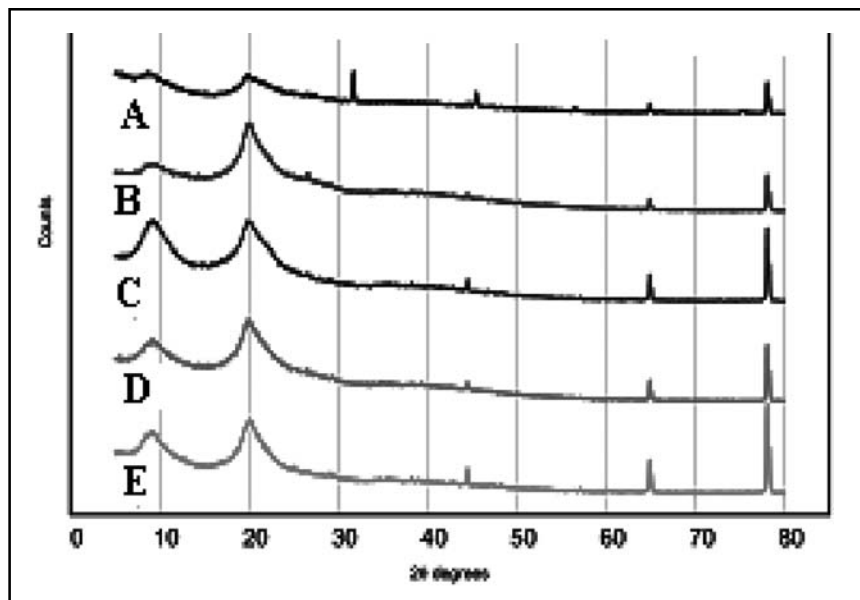Fig. 1. FT-IR spectra of CH and CH/POSS nanocomposite film samples.

Fig. 2. XRD patterns of CH and CH/POSS composite samples

evident [Figure 3(d-e)]. This might be due to the even distribution of POSS in the polymer matrix as well as good compatibility of the nanoparticles with the polymer matrix. Besides, small voids and holes were observed in the films containing 3.0 or 5.0 wt. % of POSS filler. These holes in the polymer matrix were probably created by the air that adhered on the irregular surfaces of the POSS.

The morphology of the nanocomposite films were also studied by TEM analysis. The TEM micrographs of CH film and the fractured surface of CH/POSS nanocomposite are shown in Figure 4. The morphology of CH film is smooth and uniform with no specific features while that of the nanocomposite film suggests the presence of a uniform dispersion of POSS in CHs quite good. The POSS particles can be seen in the form of extended spherical particles with size in the range of 55 nm. This is in contrast to the morphology of the film surface observed through SEM, which suggested the formation of thick polymer layer around the filler particles at the air-film interface. The improvement in the properties of the polymer filled with nanoparticles depends critically on the available polymer–filler interfacial surface area, which is affected by both the degree of loading and the size of the filler. The particle size of POSS being in the 50 nm range the TEM image suggests that CH/POSS nanocomposite can be expected to have a large interfacial surface area and hence better mechanical properties than pure CH. The POSS particles in the nanocomposites appeared to exhibit extended spherical shape.

Thermal Properties

DSC curves of PBAT and its nanocomposites with different compositions of POSS are presented in Figure 5. The nanocomposite films
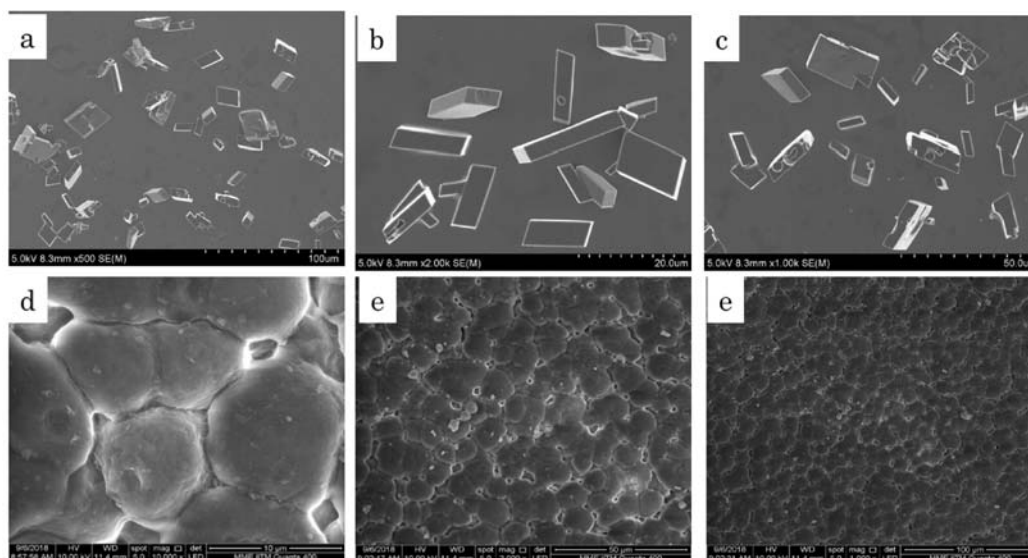

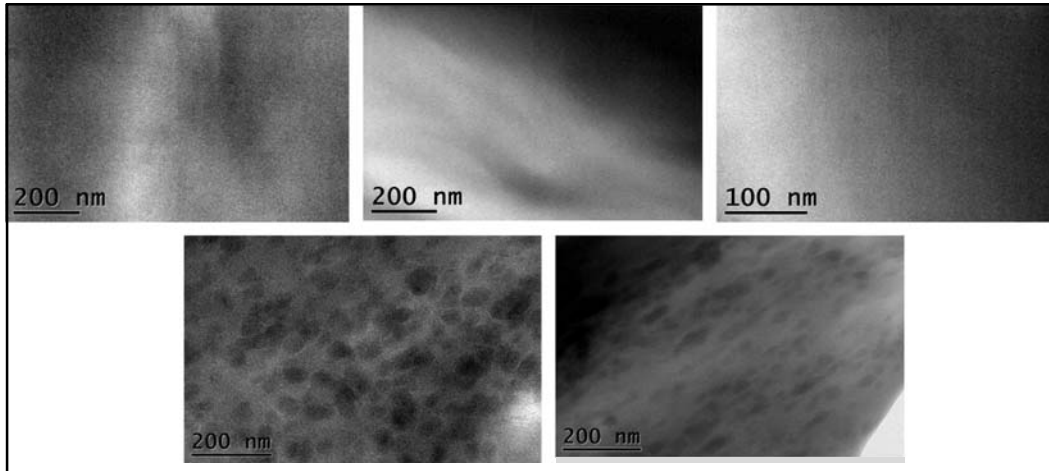Fig. 3. SEM images of POSS (a-c) and CH/ POSS nanocomposites (d-e).

Fig. 4. TEM images of (a-c) CH, (d) CH/POSS

showed melting in the range of 125-150 °C, The addition of POSS caused no significant differences in the values of T_g when compared to pure CH film. This is consistent with the observations made from FTIR spectra data that suggested no significant interaction between CH matrix and POSS filler. The TGA data for CH and all the nanocomposites are shown in Figure 6. From this, the temperature at 10% weight loss and char yield at 700 °C were obtained and used as criteria for the evaluation of thermal stability. From this data, CH/POSS nanocomposite 10.0 wt% showed better thermal stability than those containing 1.0 and 3.0 wt. % POSS. The results are consolidated in Table II. From the results, it can be seen that the addition of POSS significantly increases the temperature at 10% weight loss compared to CH. The initial decomposition temperature of the neat CH was about 375 °C while it was slightly higher for the nanocomposites. This can be explained by high heat resistance of POSS. This material acts as thermal barrier heat sink and enhances the thermal stability.

TABLE 2. Mechanical properties of CH and CH/POSS composite samples

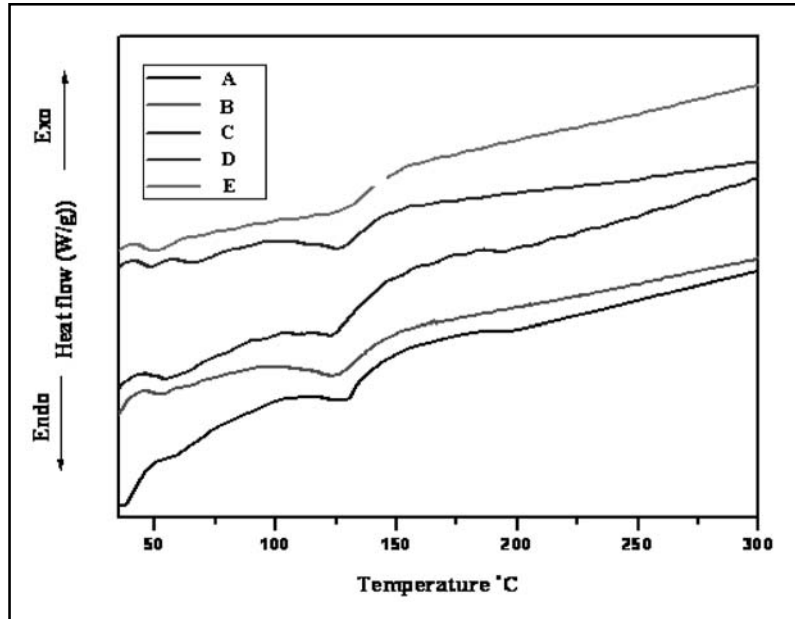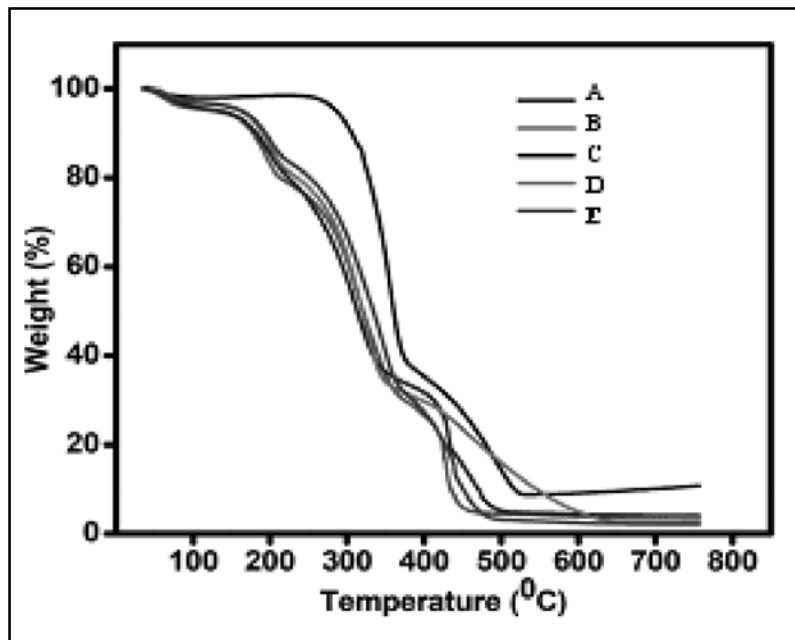| S. No	Samples Name	Thickness (μm)	Tensile strength (MPa)	Tensile modulus (MPa)	Elongation at break (%)
1.	A	65.0	10.9	2.56	675.0
2.	B	66.8	12.8	2.70	598.1
3.	C	67.1	21.3	3.01	514.9
4.	D	70.3	24.0	3.35	472.5
5.	E	75.9	6.9	4.25	389.3

Fig. 5. DSC thermo-grams of CH and CH/POSS composites

Fig. 6. TGA curves of CH and CH/POSS composite samples.

Mechanical Properties

The Mechanical properties are summarized in Table 2. It is evident from this that the addition of POSS caused significant differences in the values of tensile strength when compared to pure CH film. The tensile strength increased from 10.9 MPa in the films without POSS to 24 MPa in films with 5.0 wt. % of POSS. However, the Young's modulus was not affected as a result of filler loading. This suggests that the filler functions as a barrier in the plastic flow region in which the entanglement density is reduced as a result of the flow of the rubbery regions of CH. The elongation at break for CH film was 675% while it is reduced drastically in the case of 5.0 wt. % (D) of POSS filled CH to 327%.

Barrier Properties

Water Vapour Permeability

Water vapour permeability (WVP) values were obtained for CH and CP nanocomposites. WVP values obtained for CH and CH/POSS nanocomposite films are shown in Figure 7 (a). The WVP for A, B, C, D and E were determined to be 27.0, 38.9, 45.2, 51.0 and 59.5 g/m^2day, respectively. WVP decreased with increase in concentration of POSS in CH. The decrease in WVP could be due to the functioning of the filler particles as obstacles around which diffusion of water has to take place. Thus POSS particles increased the tortuosity of the path for the transfer of water molecules, decreasing WVP.
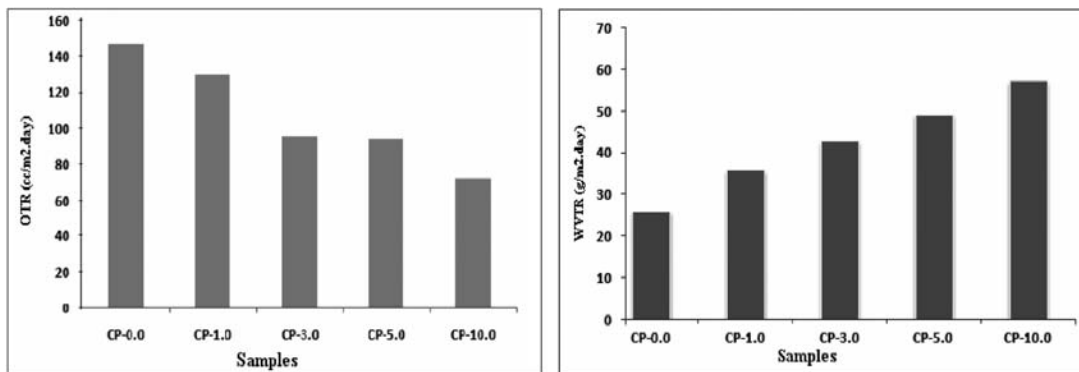

Fig. 7. Water vapour permeability (WVP) and Oxygen transmission rate (OTR) measurements for CP-0.0 and CP-1.0, CP-3.0, CP-5.0 and CP-10.0 nanocomposite films.

Oxygen Transmission Rate

Oxygen transmission rate (OTR) values obtained for PBAT and PBCP nanocomposite films are depicted in Figure 7(b). The OTR for PBAT was 1011 cc/m²day atm. OTR decreased with increase in the percentages of POSS in PBAT matrix. The lowest OTR was obtained for D, which were 76.4 cc/m²day atm. OTR values decreased by about 23% for 5.0 wt% (D) POSS loaded PBAT. The reason for the same is due to increase in path length for diffusion. Thus, PBAT containing POSS show reduction in WVP and OTR due to tortuosity of the path for diffusion of water and oxygen across the film membrane.

Wettability Measurements for PBAT nanocomposites

Water contact angle (CA) or wettability measurements were performed to examine the surface properties of CH/POSS nanocomposites and access the effect of the filler content. The representative images of CA measurements using distilled water as the probe liquid is shown in Figure 8. The CA for
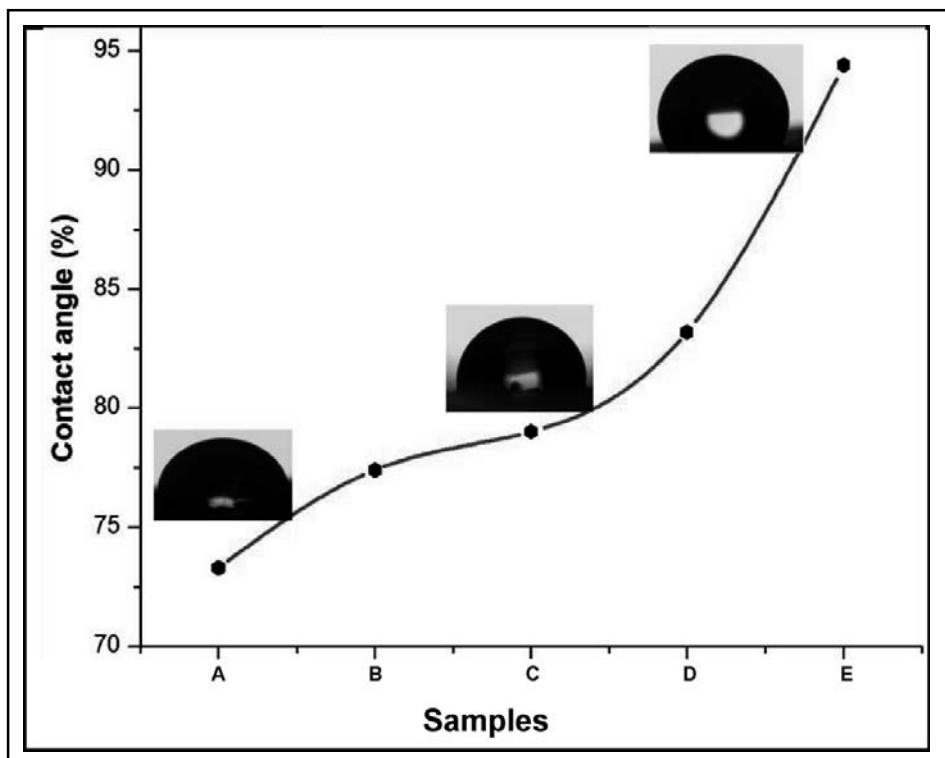

Fig. 8. Water contact angle (advancing) measurements for CH and CH/POSS nanocomposite films with different weight percentage of filler.

TABLE 3. Zone inhibition of (NPs) at different concentrations for *E.coli*

S. No.	POSS filler (Wt. %)	Zone of inhibition (mm)
1.	0	11.3
2.	1	11.8
3.	3	12.6
4.	5	13.5
5.	10	14.2

neat CH is 73° attesting to its hydrophobic nature. This increased dramatically with increasing POSS content indicating not only an increase in the hydrophobic character (due to presence of dangling propyl and silica groups borne by the filler) of the material but also that the filler is present at the film-air interface. Earlier, similar result was reported for nanocomposites of CH filled with increasing nanoclay content (hydrophilic filler; Chen *et al.,* 37 have observed similar results and found that the water CA).

Antimicrobial activity

The result of the antibacterial activity of (NPs) against *E.coli*, zone inhibition diameter for the microorganism is shown in table 1. At 10.0 concentrations (NPs) shows an excellent antibacterial activity against *E.coli*. In this present study an attempt was made to evaluate the antibacterial activity of (NPs) against *E.coli* microorganism. Based on this study, the following observations were made in Table 3.

CONCLUSIONS

Flexible, mechanically stronger and bacteria inhibiting CH films are prepared by using POSS as the filler. The most suitable filler loading is found to be 5 wt.%. The anti-bacterial activity of the films is attributed to the concentration of POSS filler at the film-air interface. The TEM studies of fractured films indicated that POSS particles were dispersed rather homogeneously in the CH matrix at nanoscales. The CH/POSS composite films possess better mechanical properties and thermal stability than pure PBAT film. The results suggested that the composite films can be used as food packaging materials to extend the shelf-life of packaged foods. Furthermore, the CH/POSS composite films exhibited strong antimicrobial activity against gram-negative (*E. coli*) food-borne pathogenic bacteria.

REFERENCES

1. M. Wojtczak, S. Dutkiewicz, A. Galeski, E. Piorkowska, *Eur. Polym. J.* 2014, *55*, 86.

2. M. P. Arrieta, J. Lopez, A. Hernandez, E. Rayon, *Eur. Polym. J.* 2014, *50*, 255.

3. A. Mohapatra, S. Mohanty, S. K. Nayak, *J. Polym. Environ.* 2014, *22*, 398.

4. J. W. Rhim, H. M. Park, C. S. Ha, *Prog. Polym. Sci.* 2013, *38*, 1629.

5. D. Klemm, B. Heublein, H. P. Fink, A. Bohn, *Angew. Chem. Int. Ed, 2005,44,*3358.

6. Y. Habibi, L. A. Lucia, O. J. Rojas, *Chem. Rev.* 2010,*110,* 3479.

7. A. Dufresne, *Mater. Today* 2013,*16,* 220.

8. M. A. S. Azizi Samir, F. Alloin, A. Dufresne, *Biomacromole.* 2005, *6,* 612.

9. R. V. Nonato, P. E. Mantelatto, C. E. V. Rossell, *Appl. Microbiol. Biotechnol,* 2001, *57,* 1.

10. M. N. Ravi Kumar, *React. Funct. Polym,* 2000, *46,* 1.

11. R. S. Blackburn, *Environ. Sci. Technol.* 2004, *38,* 4905.

12. A. K. Mohanty, M. Misra, L. T. Drzal, *J. Polym. Environ.* 2002, *10,* 19.

13. C. H. Goh, P. W. S. Heng, L. W Chan, *Carbohydr. Polym.* 2012, *88,* 1.

14. R. Venkatesan, N. Rajeswari, *Polym. Adv. Technol.* 2017, *28,* 1699.

15. F. Wang, X. Lu, C. He, *J. Mater. Chem.* 2011, *21,* 2775.

16. D. Gnanasekaran, K. Madhavan, B. S. R. Reddy, *J. Sci. Ind. Res.* 2009, *68,* 437.

17. B. Govindaraj, P. Sundararajan, M. Saroja devi, *Polym. Int.* 2012, *61,* 1344.

18. C. M. Leu, G. M. Reddy, K. H. Wei, *Chem. Mater.* 2003, *15,* 2261.

19. R. Venkatesan, N. Rajeswari, A Tamilselvi, *Polym. Adv. Technol.* 2018, *29,* 61.

20. R. Venkatesan, N. Rajeswari, *Polym. Adv. Technol.* 2017, *28,* 20.

21. R. Venkatesan, T. T. Thendral, N. Rajeswari, *Bull. Mate. Sci.* 2017, *40,* 609.

22. R. P. H. Brandelero, M. V. Grossmann, F. Yasashita, *Carbohydr. Polym.* 2012, *90,* 1452.

23. L. Bastarrachea, S. Dhawan, S. S. Sablani, J. Powers, *J. Food Eng.* 2010, *100*, 93.

24. E. Vijayakumar, D. Sangeetha, *Journal of Power Sources,* 2018, 375, 412-420.

25. G. Guo, C. Zhang, Z. Du, W. Zou, H. Tian, A. Xiang, H. Li, *Ind. Crops Prod.* 2015, *74*, 731.

26. R. Muthuraj, M. Misra, A. K. Mohanty, *J. Appl. Polym. Sci.* 2015, *132*, 1.

27. J. T. Yeh, C. H. Tsou, C.Y. Huang, K. N. Chen, C. S. Wu, W. L. Chai, *J. Appl. Polym. Sci.* 2010, *116,* 680.

28. E. Pollet, C. Delcourt, M. Alexandre, P. Dubois, *Eur. Polym. J.* 2006, *42*, 1330.

29. K. Fukushima, M. H. Wu, S. Bocchini, A. Rasyida, M. C. Yang, *Mate. Sci. Eng. C* 2012, *32*, 1331.

30. R. Al-Itry, K. Lawnawar, A. Maazouz, *Eur. Polym. J.* 2014, *58*, 90.

31. K. Fukushima, A. Rasyida, M. C. Yang, *Appl. Clay Sci.* 2013, *8081*, 291.

32. L. Bastarrachea, S. Dhawan, S. S. Sablani, J. H. Mah, D. H. Kang, J. Zhang, J. Tang, *J. Food Sci.* 2010, *75*, 215.

33. R. P. H. Brandelero, M. V. Grossmann, F. Yasashita, *Carbohydr. Polym.* 2012, *90,* 1452.